# Single-molecule magnet Mn_{12} on graphene

Xiang-Guo Li, James N. Fry, and Hai-Ping Cheng

Phys. Rev. B **90**, 125447 — Published 29 September 2014

DOI: 10.1103/PhysRevB.90.125447

# Single-molecule magnet $Mn_{12}$ on graphene

Xiang-Guo Li,[1,2] James N. Fry,[1] and Hai-Ping Cheng[1,2*]
[1]*Department of Physics and* [2]*The Quantum Theory Project, University of Florida, Gainesville, FL 32611*

We study energetics, electronic and magnetic structures, and magnetic anisotropy barriers of a monolayer of single-molecule magnets (SMM), $[Mn_{12}O_{12}(COOR)_{16}](H_2O)_4$ (abbreviated as $Mn_{12}$, with R=H, $CH_3$, $C_6H_5$ and $CHCl_2$), on a graphene surface using spin-polarized density-functional theory with generalized gradient corrections and the inclusion of van der Waals interactions. We find that $Mn_{12}$ molecules with ligands -H, -$CH_3$, and -$C_6H_5$ are physically adsorbed on graphene through weak van der Waals interactions, and a much stronger ionic interaction occurs using a -$CHCl_2$ ligand. The strength of bonding is closely related to the charge transfer between the molecule and the graphene sheet and can be manipulated by strain in the graphene; specifically, tension enhances *n*-doping of graphene and compression encourages *p*-doping. The magnetic anisotropy barrier is computed by including the spin-orbit interaction within density-functional theory. The barriers for the $Mn_{12}$ molecules with ligands -H, -$CH_3$ and -$C_6H_5$ on graphene surfaces remain unchanged (within 1 K) from those of isolated molecules because of their weak interaction, and a much larger reduction (10 K) is observed when using the -$CHCl_2$ ligand on graphene due to a substantial structural deformation as a consequence of the much stronger interaction. Neither strain in graphene nor charge transfer affects the magnetic anisotropy barrier significantly. Finally, we discuss the effect of strong correlation in the high spin state of a $Mn_{12}$ SMM and the consequence in SMM-surface adsorption.

## I. INTRODUCTION

Graphene has been widely studied as a promising candidate for applications in electronics,[1] spintronics,[2] and nanomechanics[3] due to its fascinating electrical and mechanical properties. Its one-atom-thick-layer structure makes graphene, with a point Fermi surface and linear dispersion band structure near the Fermi level, an ideal material for creating ultrasensitive probes and opens up an avenue to investigate proximity effects and chemical functionalization. Particularly, it has been reported that graphene-metal interfaces or molecular functionalization can induce superconductivity,[4,5] band gaps,[6] and novel magnetic patterns.[7,8]

In the last decade, single-molecule magnets (SMMs) have also attracted much attention due to their exotic magnetic properties, which are of fundamental importance and with potential application in information storage devices,[9] spin-based devices,[10] and quantum computation.[11] Among thousands of synthesized SMMs, one class, $[Mn_{12}O_{12}(COOR)_{16}](H_2O)_4$ (with R=$CH_3$), abbreviated as $Mn_{12}$, is the most widely investigated because of its large magnetic anisotropy barrier (MAB).[12] $Mn_{12}$ molecules have been synthesized with various ligands, and prior studies have showed that magnetic properties and exchange interactions of a SMM are strongly R-dependent.[13–19] To understand the effect of physical environment on properties of SMMs, especially that of a supporting substrate, it is desirable to place $Mn_{12}$ on well-defined surfaces and investigate the electronic and magnetic properties of individual molecules and monolayers. Much effort has already been made to deposit $Mn_{12}$ on various substrates, such as the metal Au(111),[20,21] the semi-metal Bi(111),[22] and even the ferromagnetic substrate Ni(111).[23] However, to our knowledge, first-principles methods have not been used to study hybrid nanoarchitectures consisting of SMMs ($Mn_{12}$) and graphitic materials. Understanding theoretically the relations among chemical composition of ligands, strain in graphene, and magnetism as well as the interactions between $Mn_{12}$ and graphene can provide important guidance for fine-tuning the properties of SMMs and graphene.

In this study, we investigate the interaction between graphene and a monolayer of $Mn_{12}$ using the density-functional theory (DFT) method.[24] The effects of ligands of $Mn_{12}$ and strains in graphene on the magnetic properties of $Mn_{12}$ and the interactions between graphene and $Mn_{12}$ are examined. Our first-principles calculations show that graphene can be *p*-doped upon adsorption by $Mn_{12}$, and the doping level as well as bonding energies are sensitive to terminating ligands in $Mn_{12}$. We also examine effects of strain in graphene on doping, adsorption energy, bonding strength, charge transfer, magnetic moment, and MAB.

The outline of this paper is as follows. The computational methods and model are described in Section II, followed by results and discussion in Section III, which focuses on the charge transfer and magnetization, bonding and binding energies as well as the magnetic anisotropy barrier. Finally, conclusions are given in Section IV.

## II. MODEL AND METHODS

We calculate electronic structure and magnetic properties of a $Mn_{12}$ monolayer on graphene within the framework of Kohn-Sham DFT[24] using the spin-polarized Perder-Burke-Ernzerhof (PBE) exchange correlation functional and projector-augmented-wave (PAW)[25,26] pseudopotentials in conjunction with the plane-wave basis as implemented in the Vienna Ab-initio Simulation Package (VASP).[27,28] The optB86b functional is chosen to include van der Waals (vdW)[29] interactions between $Mn_{12}$ and graphene. A combination of $2\times2\times1$ and $24\times24\times1$ *k*-point samplings are applied for single-point energy and density of states (DOS) calculations, respectively. The plane-wave cutoff energy is 500 eV, the energy threshold for self-consistency is $10^{-5}$ eV, and the force threshold for structure relaxation is 0.05 eV/Å. Four kinds of ligands, R=–H, -$CH_3$, -$C_6H_5$ and -$CHCl_2$ are considered in this study. To simulate a monolayer of $Mn_{12}$ molecules

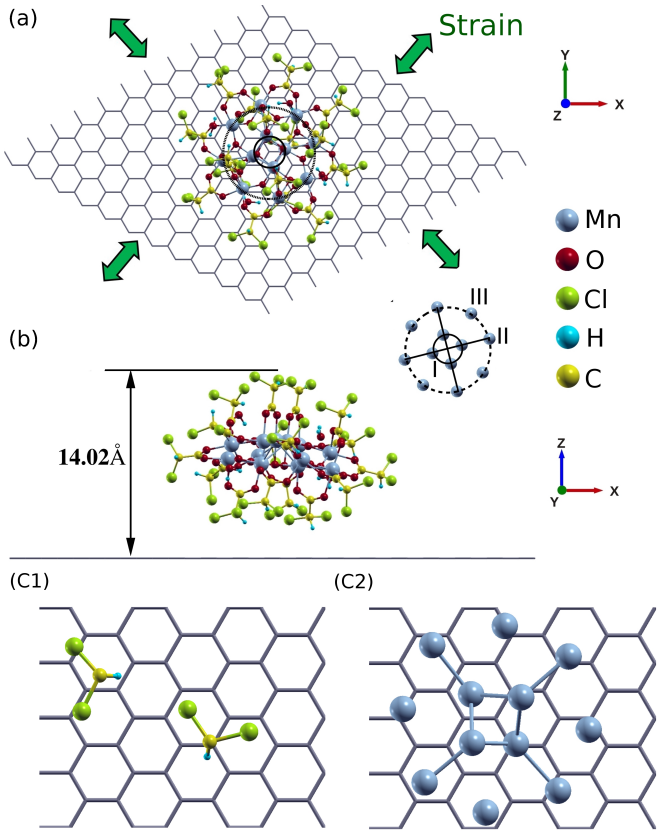


FIG. 1. (Color online) Schematic **(a)** top and **(b)** side views of a $Mn_{12}$ molecule with R=-$CHCl_2$ adsorbed onto a graphene surface. The Mn ions in three symmetry positions are denoted as I, II, and III. In supercell calculations, a vacuum layer of more than 12 Å is placed above the $Mn_{12}$ molecule. Green arrows indicate strain for both tension and compression. Strain is applied uniformly in graphene along both zigzag and armchair directions. **(c1)** Top view of two ligands in contact with graphene, and **(c2)** twelve Mn ions on graphene.

on the graphene surface (see FIG. 1), we use a 29.52 Å × 29.52 Å×30 Å hexagonal supercell (12×12 graphene primitive unit cells in the *x*-*y* plane) for the three smaller ligands R=-H, -$CH_3$, -$CHCl_2$ and a larger 31.98 Å × 31.98 Å × 32 Å hexagonal supercell (13 × 13 graphene primitive unit cells in the *x*-*y* plane) for the bigger ligand with R=-$C_6H_5$. In all cases, a vacuum layer of more than 12 Å is added above the $Mn_{12}$ molecule layer to minimize interaction between supercells. We apply a tensile strain (5%) and compressive strain (3%) to graphene by uniformly stretching or compressing graphene as illustrated in FIG. 1. The charge transfer between graphene and $Mn_{12}$ molecules and magnetization properties are analyzed using the Bader method.[30,31] The effects of the charge transfer and strains in graphene as well as the types of ligands on the MAB are analyzed from non-self-consistent spin-orbit interaction (SOI) calculations using VASP.

## III. RESULTS AND DISCUSSION

The twelve Mn ions in each $Mn_{12}$ molecule can be categorized into three classes, denoted as I, II, and III, with the four inner Mn ions belonging to symmetry class I and two sets of four Mn ions in the outer ring belonging to symmetry classes II and III (see FIG.1). The spin moments of the inner Mn ions are antiparallel (parallel) to those of the outer Mn ions in low (high) spin state. The low spin state is the ground state of the molecule, with a total magnetic moment of 20 $\mu_B$ (Bohr magneton). To find the low energy structure of $Mn_{12}$ on graphene, we first perform a set of single-point calculations with different initial configurations of $Mn_{12}$ constructed by translating or rotating $Mn_{12}$ molecules relative to graphene. From the lowest energy configuration obtained from numerous single-point calculations, we perform a geometry relaxation until the magnitudes of all force components become less than 0.05 eV/Å. In the optimized structures, the magnetic easy axis of the $Mn_{12}$ molecules (defined as the *z* axis) is very close to normal to the graphene surface. Figure 1(c1) shows the top view of two -$CHCl_2$ ligands that are in contact with the graphene and (c2) shows the twelve Mn ions on top of graphene. The average distances between the H atoms of two nearest ligands and graphene (H atoms are closest to graphene in all ligands) and between the twelve Mn ions and graphene are 2.5 Å and 8.1 Å, respectively. The values of the same quantities are 2.5 Å and 7.2 Å for ligand -H, 2.7 Å and 8.3 Å for ligand -$CH_3$, and 2.4 Å and 11.2 Å for ligand -$C_6H_5$, respectively.

### A. Charge transfer and magnetization

With the Bader method[30,31] we obtain the charges on each atom, from which we derive the charge transfer between the graphene sheet and the molecules with different ligands as well as the total magnetic moment of each sub-unit in the system, shown in FIG. 2(a). We observe that the -$CHCl_2$ ligand clearly has the largest charge transfer, followed by the -H ligand, while the -$CH_3$ and -$C_6H_5$ ligands show a much smaller charge transfer. Detailed analysis shows that the electron affinity (EA) of $Mn_{12}$ molecule is strongly dependent on the ligand type. The charge transfer is directly related to the EA of $Mn_{12}$–ligand complexes: that a $Mn_{12}$ molecule with ligand -$CHCl_2$ has the highest electron affinity (3.39 eV) due to the high electron affinity of Cl ions makes it much easier to attract electrons from graphene, and that the electron affinities of $Mn_{12}$ molecules with ligands -$CH_3$ (2.41 eV) and -$C_6H_5$ (2.39 eV) are more than 0.5 eV smaller than that with ligand -H (2.96 eV) gives rise to a much smaller charge transfer for -$CH_3$ and -$C_6H_5$. We will see later that the charge transfer modifies the magnetic moment of the magnet. Our calculation results also show that tensile strain in graphene enhances *n*-doping while compression increases *p*-doping, as seen in FIG. 2(a). The projected density of states (PDOS) of graphene confirms this conclusion. To illustrate this, we project the total density of states on graphene with an adsorbed monolayer of $Mn_{12}$ with the -$CHCl_2$ ligand, as shown in FIG. 2(b).

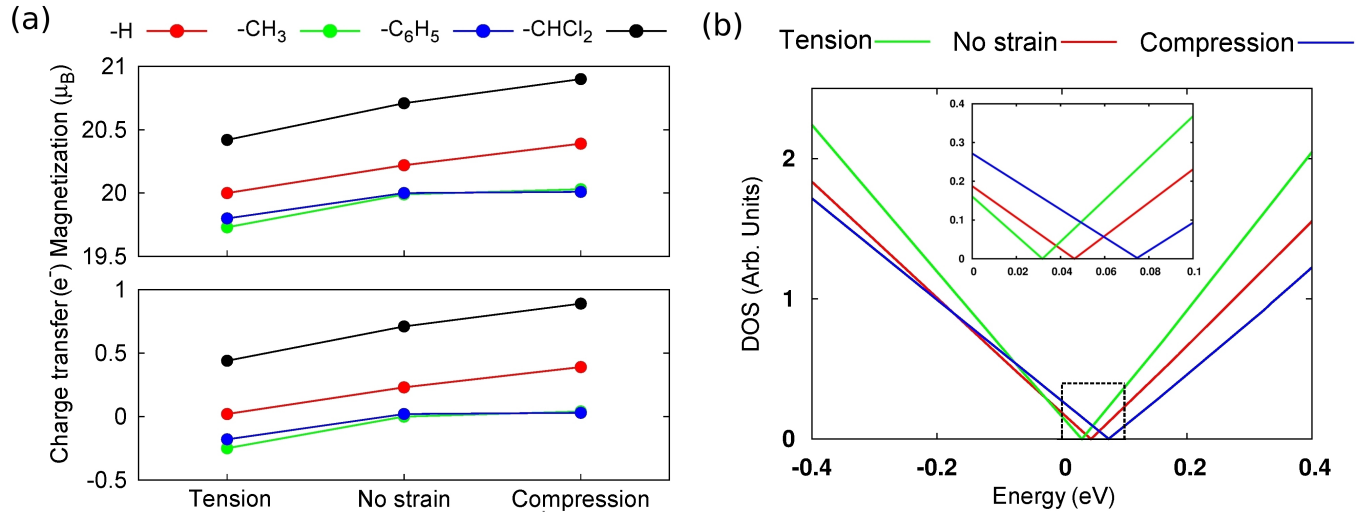


FIG. 2. (Color online) **(a)** Charge transfer between the graphene surface and $Mn_{12}$ molecules with different ligands and the total magnetic moment of the combined systems. Positive charge transfer means graphene is *p*-doped and negative means *n*-doped. Under tension, graphene has a 5% uniform tensile strain, and compression means graphene is uniformly compressed by 3%. **(b)** Projected density of state (PDOS) of graphene under different strains for ligand -$CHCl_2$.

TABLE I. Atomically resolved magnetic moments ($M$) for $Mn_{12}$ molecule with ligand -$CHCl_2$ and atomically resolved difference of the magnetic moments ($\Delta M$) between the molecule on graphene and isolated molecule in units of Bohr magneton under different kinds of strain. A positive sign in the magnetic moment change denotes an increase in the magnetic moment on the graphene surface.

| Atomic species | Initial $M$ (Isolated molecule) | $\Delta M$ (Tension) | $\Delta M$ (No strain) | $\Delta M$ (Compression) |
|---|---|---|---|---|
| Mn (I) | −9.90 | **0.12** | **0.16** | **0.18** |
| Mn (II) | 14.06 | −0.04 | 0.01 | 0.02 |
| Mn (III) | 13.89 | **0.33** | **0.40** | **0.47** |
| O, C, H | 1.90 | 0.06 | 0.13 | 0.15 |
| Cl | 0.05 | 0.01 | 0.01 | 0.01 |
| Total | 20.00 | 0.48 | 0.71 | 0.83 |

The stronger the tensile strain, the less charge transfers to the molecule. Spin density analysis shows that the trend of the total magnetization is the same as the charge transfer; that is, the magnitude of the magnetization change of the molecule upon adsorption on graphene parallels the charge transfer, which indicates that the transferring electrons are spin-up (majority) electrons. The calculated DOS of $Mn_{12}$ molecules adsorbed on graphene (e.g. with -$CHCl_2$ ligand, shown in top of FIG. 3) also testifies this, since the spin-down states (blue curve) have a big gap around the Fermi level, and all the states slightly below the Fermi level are from spin-up states (red curve).

The spin magnetic moment differences between the combined system and isolated $Mn_{12}$ molecule with the -$CHCl_2$ ligand, also calculated using Bader method, are shown in TABLE I. Relatively large magnetic moment changes in Mn(I) and Mn(III) (denoted in boldface in TABLE I) indicate that electrons from graphene are mainly transferred to Mn(I) and Mn(III) ions. In order to understand this, we plot the DOS of the combined system and the PDOS of Mn and O atoms as shown in the top panel of FIG.3. Clearly, as more electrons are transferred to the molecule, the original LUMO of the isolated molecule moves below the Fermi level, and the states just below the Fermi level are mainly contributed from Mn(I) and Mn(III) ions. We can also deduce the same conclusion from the PDOS of the isolated molecule (see the bottom panel of FIG.3), since the main contribution to the LUMO is from Mn(I) and Mn(III) ions, circled in green. The peak heights in the PDOS for the combined system are reduced and orbital energies broadened compared to the PDOS of the isolated molecules due to the interaction with the graphene surface. From TABLE I, we can also see the magnetic moment changes in the ligand, especially in the Cl ions, are much smaller than the corresponding total charge transfer, which tells us most of the transferred electrons are not ending on the Cl ions, even though the large charge transfer is due to the strong capacity of Cl atoms to gain electrons. Therefore, we conclude that two consecutive charge transfer processes occur when placing $Mn_{12}$ molecules on graphene surfaces. The Cl atoms play the role of a charge transfer bridge. The higher the electron affinity of the ligand, the larger the amount of charge transfer, indicating that the $Mn_{12}$ molecules can interact with the environment through ligands.

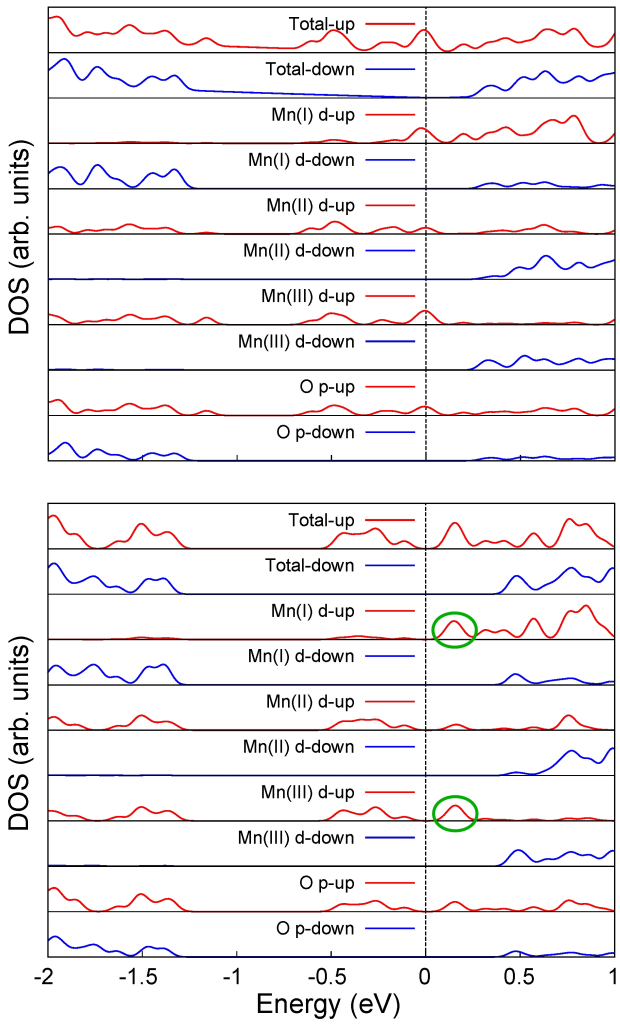


FIG. 3. (Color online) Total spin-resolved DOS and PDOS of Mn $d$ and O $p$ orbitals in a $Mn_{12}$ molecule with ligand -$CHCl_2$ adsorbed on graphene system (top) and in the isolated $Mn_{12}$ molecule with ligand -$CHCl_2$ (bottom). The total DOS for both spin-up and spin-down are scaled by a factor of $\frac{1}{3}$ for the combined system (top) and a factor of $\frac{1}{2}$ for the isolated molecule (bottom). The zero of energy denotes the Fermi level for the combined system and the midpoint between the highest occupied molecular orbital (HOMO) and the lowest unoccupied molecular orbital (LUMO) for the isolated molecule system. The smearing parameter is $\sigma = 0.05$ eV.

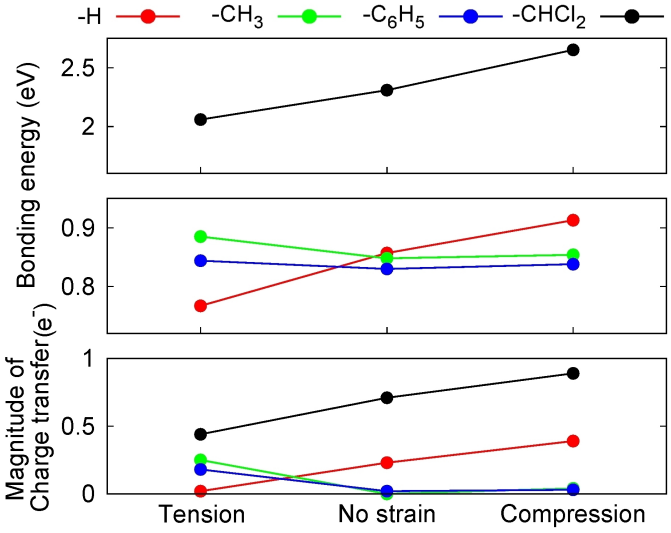


FIG. 4. (Color online) Bonding energy of $Mn_{12}$ with different ligands adsorbed on graphene surface and the magnitude of charge transfer between the graphene surface and the molecule.

### B. Bonding and binding energies

For different ligands and at various strains we compute bonding energies and binding energies $E_b$ between $Mn_{12}$ and graphene as

$$E_b = E_{\text{graphene}} + E_{\text{molecule}} - E_{\text{molecule+graphene}}. \quad (1)$$

For bonding energy calculations in Eq. (1), geometries of a molecule and the graphene are kept the same as in the adsorbed state; for binding energy, we let both graphene and molecule relax to their optimal structures in separation. Bonding energy measures the strength of the bond between the molecule and graphene, whereas the binding energy measures the overall energy gain when the molecule and the graphene join together. By this definition, one expects the absolute value of bonding energy to be greater than that of binding energy. To relate bonding energies to charge transfer between the molecule and graphene, we plot the bonding energy and the magnitude of charge transfer together as functions of strain (FIG. 4). The trend of bonding energies follows that of charge transfer magnitude for all four ligands, which indicates that charge transfer is a major factor influencing the bonding energy in these systems. The bonding energies for ligands -H, -$CH_3$ and -$C_6H_5$ vary from 0.7 eV to 1.0 eV, which indicates that the interactions between the molecule and graphene is vdW in nature. For the ligand -$CHCl_2$, the bonding energy can be as high as 2.7 eV; this interaction should be a relatively weak ionic bonding.

Through examining the calculated binding energies, we can also obtain hints about the nature of interactions between the molecule and the graphene surface. For the weaker vdW interaction, compared to the bonding energies the binding energies are lowered only by 0.023 eV, 0.018 eV, and 0.023 eV for ligands -H, -$CH_3$ ,and -$C_6H_5$, respectively, and molecular structures and electronic properties are only slightly changed upon adsorption. For the ligand -$CHCl_2$, the binding energy decreases by as much as 1.149 eV, and the molecule undergoes a much larger change in structure and electronic properties. A much stronger chemical interaction exists in this case.

### C. Magnetic anisotropy barrier

It is known that the Jahn-Teller distortion among the eight $Mn^{3+}$ ions in the outer ring gives the the magnetic anisotropy of $Mn_{12}$.[32,33] We investigate the MAB by computing the the total energy for a rotation of the spin axis from the $z$-direction

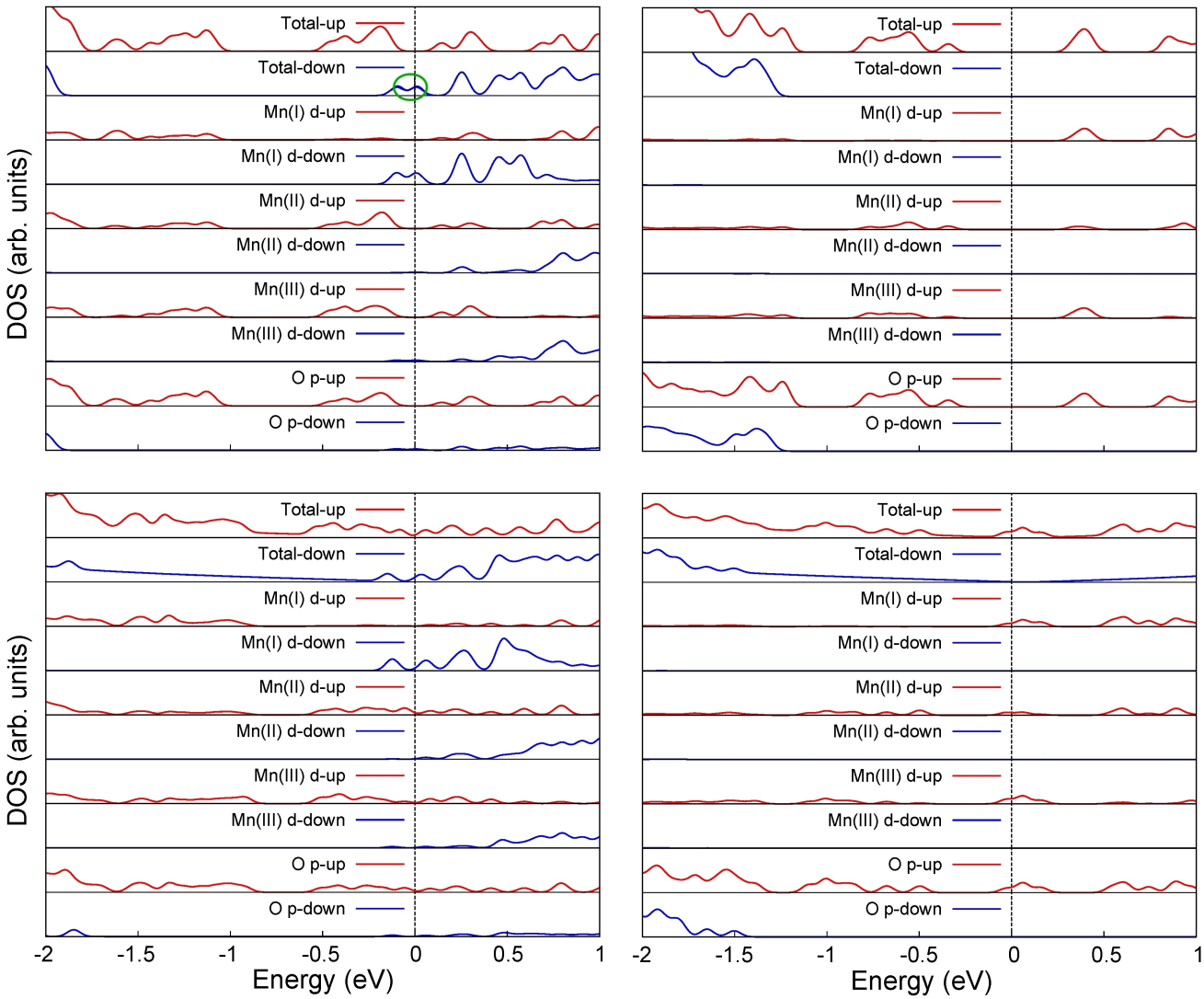


FIG. 5. (Color online) Total spin-resolved DOS and PDOS of Mn $d$ and O $p$ orbitals in an isolated high-spin state $Mn_{12}$ molecule with ligand -$CHCl_2$ (top row) and in the molecule adsorbed on graphene (bottom row) from GGA calculations (left column) and GGA+$U$ calculations (right column). Again, the total DOS is scaled by a factor of $\frac{1}{3}$ for the combined system and $\frac{1}{2}$ for the isolated molecule. The zero of the horizontal scale denotes the midpoint between HOMO and LUMO for isolated molecules (top row) and the Fermi level for molecules adsorbed on graphene (bottom row). The smearing parameter is $\sigma = 0.05$ eV.

to the $x$-$y$ plane using a non-self-consistent SOI calculation. The goal is to understand the effects of the supporting graphene on the MAB. As shown in TABLE II, our barriers for isolated $Mn_{12}$ molecules with different ligands are between 60 K and 70 K, in agreement with all-electron calculations[34] and experimental values.[35] In addition, we examine the in-plane ($x$-$y$ plane) preference of the spin axis, and our calculations show that the energy variation is within 1 K for different directions. Adsorbed on graphene, the MAB shows very little change for $Mn_{12}$ molecules terminated by -H, -$CH_3$, and -$C_6H_5$ (reductions of order ∼1 K) as a result of the weak interaction. For the -$CHCl_2$ terminated molecule, the MAB is reduced by about 10 K, or ∼17%, due to the stronger interaction. We note that -H terminated $Mn_{12}$ does not show more reduction in barrier height than the other two ligands with vdW interactions.

We also compute the MAB of isolated molecule with geometry as taken directly from the combined system without relaxation, the same as for bonding energy calculations. Through comparison of the MAB for the isolated molecules before and after relaxation, we can separate the effects of structure change from charge transfer on the MAB. For vdW interaction ligands -H, -$CH_3$ and -$C_6H_5$, structure change is very small, confirmed by the small differences between bonding and binding energies, making the MAB almost the same. For -$CHCl_2$ terminated molecule, the structural change results in a 5.6 K reduction in MAB, followed by a 3.5 K further reduction due to the sizable charge transfer. We conclude that structural de-

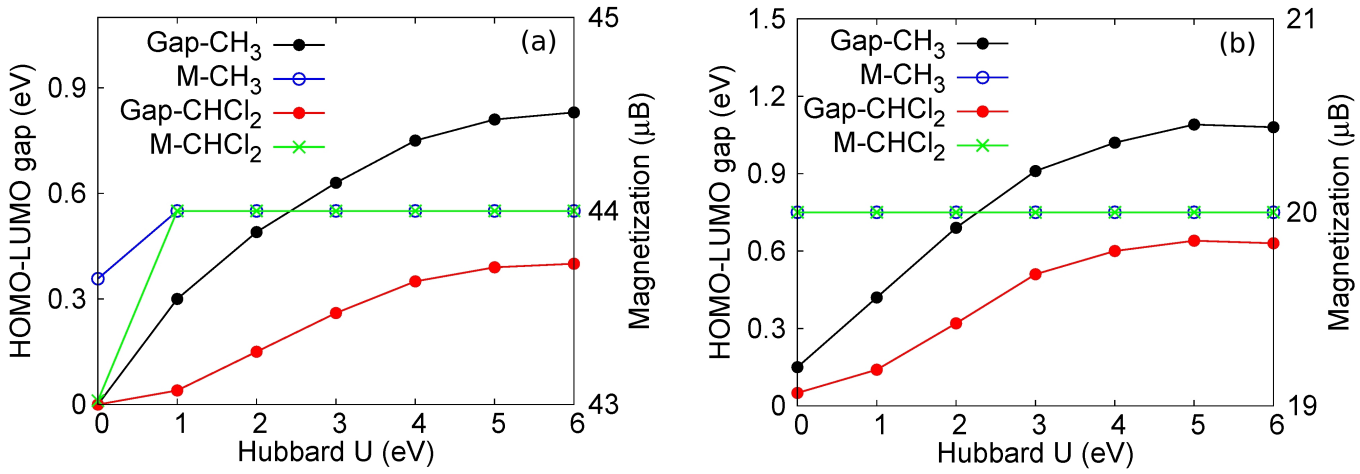


FIG. 6. (Color online) The HOMO-LUMO gap and total magnetization (M) as a function of the Hubbard $U$ values for isolated $Mn_{12}$ molecule with ligand -$CHCl_2$ and -$CH_3$ in **(a)** high-spin and **(b)** low-spin states.

formation has stronger effect on MAB than charge transfer, which explains why MAB changes so little for -H terminated molecule, in spite of the non-zero charge transfer. Moreover, we investigate the effect of strain on MAB. Our results show that strains in graphene have little effect on the structure or the MAB of $Mn_{12}$ molecules, which again indicates that the charge transfer is not a major factor on MAB of $Mn_{12}$ in our systems (although strain does affects charge transfer).

Finally, with regard to the ligand effects on the MAB in the $Mn_{12}$ molecule, we find that when a molecule is isolated the barrier height does not change much (a range of $\sim 6.1$ K) with different ligands. When the molecule adsorbed on graphene, the difference in MAB increases to $\sim$15 K due to the rearrangement of charges. The charge arrangement caused by the graphene substrate in this work is much smaller than that by a gold substrate. O'Shea *et al.* have observed a significant charge transfer between gold and a monolayer of $Mn_{12}$ molecules even with the more protective large -$C_6H_5$ ligand.[36] In this case, the MAB should be strongly affected by the ligand types due to the much more dramatic rearrangement of charge.

TABLE II. Magnetic anisotropy barriers for isolated and graphene-supported $Mn_{12}$ molecules with different ligands, in units of K.

| | -H | -$CH_3$ | -$C_6H_5$ | -$CHCl_2$ |
|---|---|---|---|---|
| Isolated molecule | 63.4 | 62.7 | 67.3 | 61.2 |
| Graphene-supported | 62.7 | 61.5 | 66.1 | 51.1 |
| Isolated molecule (w/o relaxation) | 63.3 | 62.2 | 66.9 | 55.6 |

### D. High-spin states

Before concluding, we make a few comments on the high-spin states of $Mn_{12}$ molecules on graphene. Although the high-spin state is not the ground state spin configuration, the transition from the low-spin state to the high-spin state can be controlled, in principle, by magnetic field, and such spin-state switching leads to the concept of molecular magneto-capacitance.[37] In the high-spin state, an isolated $Mn_{12}$ molecule with $CHCl_2$ as the ligand has a total magnetic moment of $44\,\mu_B$. By performing generalized gradient approximation (GGA) calculations, we find that there are spin-down states around Fermi level in the PDOS of Mn(I), circled in green, as shown in top left of FIG. 5. As a result, the electrons transferred to the molecule from graphene occupy both spin-up and spin-down orbitals, which can be observed from the PDOS of the combined system (see bottom left of FIG. 5). Thus the change of the magnetization of the molecule upon adsorption on graphene no longer follows the same trend as the charge transfer. The GGA calculations on $Mn_{12}$ molecule with ligand -$CHCl_2$ adsorbed on graphene show that the charge transfer from graphene to the molecule is 0.75 electrons, while the magnitude of magnetization change is $-0.43\,\mu_B$. Nevertheless, the peak of the spin-down DOS at the Fermi surface suggests that the system might be highly correlated, and calculations beyond the GGA exchange-correlation potential may be needed to properly treat the Coulomb interaction in the localized $d$ states. To examine the effects of strong correlation, we apply the GGA+$U$ method[38] to the $Mn_{12}$ molecule with ligand -$CHCl_2$ adsorbed on graphene system with $U$=4 eV for the Mn $d$ orbitals. This value of $U$ was selected in order to reproduce photoemission spectra measured for a crystal of $Mn_{12}$ molecules.[39]. Our GGA+$U$ calculations show a large gap for the spin-down channel, similar to the low-spin state in the PDOS of Mn(I) (see top right of FIG. 5). Therefore, electrons transferred to the molecule should still be spin-up electrons in the high-spin state, which is confirmed by the PDOS of the

combined system (see bottom right of FIG. 5). The results that the charge transfer is 0.95 electrons and the magnitude of the magnetization change is $+0.96\,\mu_B$ with GGA+$U$ calculations indicate that GGA and GGA+$U$ lead to different physical pictures. To further elaborate the $U$-dependence, we perform a systematic study for isolated $Mn_{12}$ (terminated by -$CHCl_2$ and -$CH_3$) in both high-spin and low-spin states. For the high-spin state, as discussed above, the emergence of the spin-down state around Fermi level when $U = 0$ closes the HOMO-LUMO gap and reduces the total molecule spin. The Hubbard $U$ introduces a finite HOMO-LUMO gap in the molecule, and the total molecule spin becomes $44\,\mu$B and stays unchanged for $U = 1$–$6$ eV, as shown in FIG. 6(a). For the low-spin state, the molecule always has a finite HOMO-LUMO gap and the total spin is $U$-independent [see FIG. 6(b)], which agrees with previous studies.[40,41] We also find that the HOMO-LUMO gap increases monotonically and then saturates around $U = 5$–$6$ eV, and the HOMO-LUMO gap for ligand -$CHCl_2$ is consistently smaller than that for ligand -$CH_3$. The $\sim$1 eV HOMO-LUMO gap at $U = 4$ eV for ligand -$CH_3$ in low-spin state matches the experimental value.[40,42]

As for the low spin states, GGA+$U$ calculations do not show much difference in the electronic properties discussed in previous sections, since both GGA and GGA+$U$ calculations give a large gap for the spin-down channels. The same conclusion, that DFT+$U$ calculations show results similar to GGA calculations for $Mn_{12}$ low spin states, has also been made for $Mn_{12}$ adsorption on a Ni(111) surface.[23] These differences between the $Mn_{12}$ low-spin results and the high-spin states discussed above are probably due to stronger correlation in the high-spin state.[43]

## IV. CONCLUSION

Using first-principles calculations, we have studied the interactions between a monolayer of single-molecule magnets, $[Mn_{12}O_{12}(COOR)_{16}](H_2O)_4$ with R=-H, -$CH_3$, -$C_6H_5$ and -$CHCl_2$, and graphene. Our results show that $Mn_{12}$ with ligands -H, -$CH_3$, -$C_6H_5$ are weakly adsorbed on graphene, through the vdW interaction; however, the interaction is much stronger and ionic in nature for the ligand -$CHCl_2$. The calculated bonding energy is closely related to the charge transfer between molecules and graphene, and both are also correlated with strains applied to the graphene. Specifically, a tensile strain can enhance $n$-doping of graphene, while compression of graphene will increase $p$-doping. Our SOI calculations suggest a slight decrease in MAB for weakly interacting $Mn_{12}$ with ligands -H, -$CH_3$ and -$C_6H_5$, but a much larger reduction in MAB, about 17%, is observed for the strong interacting systems involving $Mn_{12}$ with ligand $CHCl_2$. A relatively larger structure change in the $Mn_{12}$ molecules on adsorption plays an important role in the large MAB reduction, which is also confirmed by the large binding energy decrease compared to the bonding energy for the ligand -$CHCl_2$. Surprisingly, applied strain and charge transfer are not major factors in MAB. Our results and analysis in this study clearly elaborate the effects of ligands in $Mn_{12}$ SMMs and of strains in graphene, which provide new avenues for experimental studies and application design involving SMMs and graphene.

### Acknowledgements

This work was supported by the US Department of Energy (DOE), Office of Basic Energy Sciences (BES), under Contract No. DE-FG02-02ER45995. The computation was done using the utilities of the National Energy Research Scientific Computing Center (NERSC).

* Email: cheng@qtp.ufl.edu; Tel: 352-392-6256


[1] A. H. Castro Neto, F. Guinea, N. M. R. Peres, K. S. Novoselov, and A. K. Geim, Rev. Mod. Phys. **81**, 109 (2009).

[2] N. Tombros, C. Jozsa, M. Popinciuc, H. Jonkman, and B. van Wees, Nature. **448**, 571 (2007).

[3] J. S. Bunch, A. M. van der Zande, S. S. Verbridge, I. W. Frank, D. M. Tanenbaum, J. M. Parpia, H. G. Craighead, and P. L. McEuen, Science **315**, 490 (2007).

[4] B. M. Kessler, C. O. Girit, A. Zettl, and V. Bouchiat, Phys. Rev. Lett. **104**, 047001 (2010).

[5] H. Heersche, P. Jarillo-Herrero, J. Oostinga, L. K. Vandersypen, and A. Morpurgo, Nature. **446**, 56 (2007).

[6] D. C. Elias, R. R. Nair, T. M. G. Mohiuddin, S. V. Morozov, P. Blake, M. P. Halsall, A. C. Ferrari, D. W. Boukhvalov, M. I. Katsnelson, A. K. Geim, and K. S. Novoselov, Science **323**, 610 (2009).

[7] A. V. Krasheninnikov, P. O. Lehtinen, A. S. Foster, P. Pyykkö, and R. M. Nieminen, Phys. Rev. Lett. **102**, 126807 (2009).

[8] Y. S. Dedkov, M. Fonin, U. Rüdiger, and C. Laubschat, Phys. Rev. Lett. **100**, 107602 (2008).

[9] C. Joachim, J. K. Gimzewski, and A. Aviram, Nature. **408**, 541 (2000).

[10] C. Timm and F. Elste, Phys. Rev. B **73**, 235304 (2006).

[11] M. Leuenberger and D. Loss, Nature. **410**, 789 (2001).

[12] A. L. Barra, D. Gatteschi, and R. Sessoli, Phys. Rev. B **56**, 8192 (1997).

[13] R. Sessoli, H. L. Tsai, A. R. Schake, S. Wang, J. B. Vincent, K. Folting, D. Gatteschi, G. Christou, and D. N. Hendrickson, Journal of the American Chemical Society **115**, 1804 (1993).

[14] N. E. Chakov, S.-C. Lee, A. G. Harter, P. L. Kuhns, A. P. Reyes, S. O. Hill, N. S. Dalal, W. Wernsdorfer, K. A. Abboud, and G. Christou, Journal of the American Chemical Society **128**, 6975 (2006).

[15] H.-L. Tsai, H.-A. Shiao, T.-Y. Jwo, C.-I. Yang, C.-S. Wur, and G.-H. Lee, Polyhedron **24**, 2205 (2005).

[16] H. Zhao, C. P. Berlinguette, J. Bacsa, A. V. Prosvirin, J. K. Bera, S. E. Tichy, E. J. Schelter, and K. R. Dunbar, Inorganic Chemistry **43**, 1359 (2004).

[17] S. W. Yoon, M. Heu, W. S. Jeon, D.-Y. Jung, B. J. Suh, and S. Yoon, Phys. Rev. B **67**, 052402 (2003).

[18] M. Soler, P. Artus, K. Folting, J. C. Huffman, D. N. Hendrickson, and G. Christou, Inorganic Chemistry **40**, 4902 (2001).

[19] D. W. Boukhvalov, V. V. Dobrovitski, P. Kogerler, M. Al-Saqer, M. I. Katsnelson, A. I. Lichtenstein, and B. N. Harmon, Inorganic Chemistry **49**, 10902 (2010).

[20] S. Voss, M. Fonin, U. Rüdiger, M. Burgert, U. Groth, and Y. S. Dedkov, Phys. Rev. B **75**, 045102 (2007).

[21] S. Barraza-Lopez, M. C. Avery, and K. Park, Phys. Rev. B **76**, 224413 (2007).

[22] K. Sun, K. Park, J. Xie, J. Luo, H. Yuan, Z. Xiong, J. Wang, and Q. Xue, ACS Nano **7**, 6825 (2013).

[23] K. Park, Phys. Rev. B **83**, 064423 (2011).

[24] W. Kohn and L. J. Sham, Phys. Rev. **140**, A1133 (1965).

[25] P. E. Blöchl, O. Jepsen, and O. K. Andersen, Phys. Rev. B **49**, 16223 (1994).

[26] G. Kresse and D. Joubert, Phys. Rev. B **59**, 1758 (1999).

[27] G. Kresse and J. Furthmüller, Phys. Rev. B **54**, 11169 (1996).

[28] G. Kresse and J. Furthmller, Computational Materials Science **6**, 15 (1996).

[29] J. Klimeš, D. R. Bowler, and A. Michaelides, Phys. Rev. B **83**, 195131 (2011).

[30] R. F. W. Bader, "Atoms in molecules," in *Encyclopedia of Computational Chemistry* (John Wiley & Sons, Ltd, 2002).

[31] G. Henkelman, A. Arnaldsson, and H. Jnsson, Computational Materials Science **36**, 354 (2006).

[32] R. Bagai and G. Christou, Chem. Soc. Rev. **38**, 1011 (2009).

[33] K. Park and M. R. Pederson, Phys. Rev. B **70**, 054414 (2004).

[34] M. R. Pederson and S. N. Khanna, Phys. Rev. B **60**, 9566 (1999).

[35] A. L. Barra, D. Gatteschi, and R. Sessoli, Phys. Rev. B **56**, 8192 (1997).

[36] A. Saywell, A. J. Britton, N. Taleb, M. del Carmen Gimnez-Lpez, N. R. Champness, P. H. Beton, and J. N. OShea, Nanotechnology **22**, 075704 (2011).

[37] Y.-N. Wu, X.-G. Zhang, and H.-P. Cheng, Phys. Rev. Lett. **110**, 217205 (2013).

[38] V. I. Anisimov, J. Zaanen, and O. K. Andersen, Phys. Rev. B **44**, 943 (1991).

[39] U. del Pennino, V. D. Renzi, R. Biagi, V. Corradini, L. Zobbi, A. Cornia, D. Gatteschi, F. Bondino, E. Magnano, M. Zangrando, M. Zacchigna, A. Lichtenstein, and D. Boukhvalov, Surface Science **600**, 4185 (2006).

[40] D. W. Boukhvalov, M. Al-Saqer, E. Z. Kurmaev, A. Moewes, V. R. Galakhov, L. D. Finkelstein, S. Chiuzbaian, M. Neumann, V. V. Dobrovitski, M. I. Katsnelson, A. I. Lichtenstein, B. N. Harmon, K. Endo, J. M. North, and N. S. Dalal, Phys. Rev. B **75**, 014419 (2007).

[41] D. W. Boukhvalov, A. I. Lichtenstein, V. V. Dobrovitski, M. I. Katsnelson, B. N. Harmon, V. V. Mazurenko, and V. I. Anisimov, Phys. Rev. B **65**, 184435 (2002).

[42] S. Voss, M. Fonin, U. Rüdiger, M. Burgert, U. Groth, and Y. S. Dedkov, Phys. Rev. B **75**, 045102 (2007).

[43] V. Anisimov and Y. Izyumov, *Electronic Structure of Strongly Correlated Materials* (SPRINGER SERIES IN SOLID-STATE SCIENCE 163).